Energy, daylight and thermal analysis of a geodesic dome with photovoltaic envelope

Marco Lovati, Philip Ingenhoven, Giuseppe De Michele, Luca Baglivo, Laura Maturi, David Moser

Institute for Renewable Energy, EURAC research, Viale Druso 1, 39100 Bolzano, Italy

Bolzano/Bozen, Italy, Marco.Lovati@eurac.edu

Abstract

In this paper, a unified model of the physical behaviour of a fabric structure with building integrated photovoltaics (BIPV) is proposed. The advantages of this flexible, lightweight structure will be combined with the energy harvesting properties of photovoltaic (PV) integration. The method is demonstrated on a geodesic dome with 10m radius, which is partly equipped with photovoltaic panels. This special geometry is part of a design study within the FP7 project “SolarDesign”.

The method proposed here consists of three parts, namely the energetic analysis of the PV, the daylighting influence of the opaque PV modules and finally the thermal impact of the BIPV.

As a first step, irradiance was simulated to find the optimal configuration for the PV modules on the dome by maximizing the net present value of the system over 20 years. This evaluation shows a relatively constant value of this economical parameter within a broad spectrum of configurations providing some freedom left to optimize the positioning of the PV panels. In the second step, the lighting condition inside the structure was enhanced minimizing the glare and keeping the illuminance levels at sufficient values to ensure comfort, by positioning and choosing the material of the building envelope accordingly. Finally, the thermal parameters inside the dome were examined. Here a twofold iteration scheme was used implementing finite elements analysis, first to find the boundary conditions, i.e. the temperature of the building envelope and then, using these temperatures, to find the inside temperature of the structure, which in turn influences the envelope temperature. Thus, the inside thermal condition of the geodesic dome was found iteratively. The combination of the three steps allows for an optimal configuration of BIPV modules that takes into account not only costs but also visual and thermal comfort.

Keywords: BIPV, performance simulation, daylight, computational fluid dynamics (CFD) .

1. Introduction

The presented study is an attempt to unify different aspects of building simulation. Economic, energy production, daylighting and thermal aspects of a building integrated PV (BIPV) installation are combined. The final aim is to give designers and architects a tool for BIPV planning and keep under control all the different effects that the PV installation has on the building. In the first step an economic/energetic model similar to [1] is used to define the Net Present Value (NPV) of the installation according to the irradiation potential. This generates a financially optimal range of installed nominal power. In the second step, the daylighting is considered using a method, based on RADIANCE [2] and DAYSIM [3], derived from [4][5][6]. The overall illuminance and the glare are analyzed to find and optimal solution, in which enough light enters but no distress is caused by glare. The method measures the minimum illuminance on a horizontal measuring grid, but the maximum illuminance on a set of vertical measuring points (simplified viewpoints).The third step evaluates the thermal effect of the PV installation on the building, using the finite elements (FEM) tool ELMER [7].All the software tools used are free of charge and open source. The final goal of this work is to combine these different tools in a single one to provide a detailed analysis of the complete system and give valuable support in the planning of BIPV systems.

2. Method

2.1 Electricity production optimization

All properties (energetic, daylighting and thermal) of the installation of PV modules depend on the location and quantity of modules installed; these parameters ultimately depend on the economic performance of the system; therefore, the first phase of the optimization aims to decide on which surface to put PV modules for maximum profitability over 20 years of lifetime.

2.1.1 Generation of the model

The simulation is carried at its core by the validated Radiance [2] software to estimate the annual cumulative radiation on a given surface. The method requires as inputs the followings [Table 1]:

Geometry	**PV system**	**Energy price**
Shape Location Shading scenario Materials Constraints	Efficiency Performance ratio Degradation rate Initial price Maintenance costs	Energy price Energy price growth rate

Table 1: input for production optimization

Shape is the sum of all the surfaces that are suitable for a PV module, and contains information about the area of every surface on which it is possible to integrate PV and its orientation. Constraints may be the presence of windows, vents or other regions that are unsuitable for the installation of PV. In the case presented, a geodesic

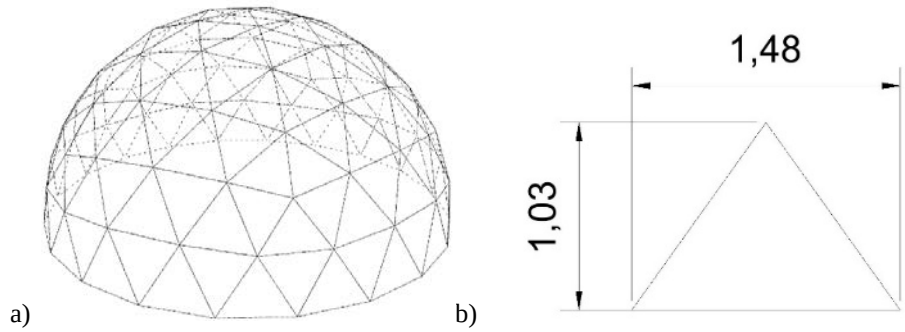

Figure 1: a) sketch of the geodesic dome b) dimensions of the PV module

dome was examined, see [Figure 1a)]. In this special building, every surface is oriented in a different way, i.e. receiving a different annual irradiation. This geometry was chosen as a case study within the SolarDesign FP7 project. The triangles in a geodesic dome are not identical. However, manufacturing PV modules with different dimensions would be very complex and costly, so only one standard size of the PV module was chosen, that fits even the smallest triangle was used, i.e. an area of 0.76 m^2 [Figure 1b] . The annual cumulative radiation [$Wh•(sr•year)^{-1}•m^{-2}$] is estimated using the Gencumulativesky routine within the Radiance suite. This forms a discrete sky vault built on a variation of the sky model proposed by [8]. Gencumulativesky calculates the position of the sun from latitude and longitude (of the location), and based on the information retrieved from a Meteonorm generated weather file it assigns a value of cumulative radiance to each sky patch. The cumulative irradiation [$Wh•year^{-1}•m^{-2}$] on the surfaces is then calculated using the Rtrace routine on a chosen set of Euclidean vectors anchored to the centroid of every surface, the radiative power entering each panel is obtained by multiplying the irradiation by the area.

2.1.2 Optimum assessment

To evaluate positioning on the dome, a threshold representing the minimum irradiation for a surface to be covered with a PV module was set. To estimate the yearly power production the following formula was used [equation 1]:

$$E_{thr} = A_{min} \cdot \eta \cdot PR \cdot \sum_{n=1}^{n_{threshold}} H_n,$$

Equation 1: annual energy production

where $\mathbf{E_{thr}}$ is the energy output [kWh] for one year, $\mathbf{n_{threshold}}$ is the number installed modules, $\mathbf{A_{min}}$ is the area of a PV module [Figure 1b], **η** is the module efficiency, **PR** is the performance ratio of the system, and $\mathbf{H_n}$ is the cumulative insolation of the $\mathbf{n^{th}}$ triangle [kWh/m2 yr].Once the power production of the system is estimated its profitability is accessed through the Net Present Value (NPV)[1] which is defined as [Equation 2].

$$NPV = \sum_{t=1}^{life} \frac{E_{thr} \cdot Cp(t) \cdot P_E(t) - m_{thr}}{(1+r)^t} - I_0,$$

Equation 2: net present value at the given year

where $\mathbf{E_{thr}}$ is energy output from [equation 1], **Cp(t)** is a coefficient of performance taking into account degradation, $\mathbf{P_E(t)}$ is the price of electricity in the given year, $\mathbf{m_{thr}}$ is the maintenance associated to the number of modules (threshold), $\mathbf{I_0}$ is the initial investment and **r** is the discount rate, a measure of the future decrease in value of present money.

2.2 Daylight optimization

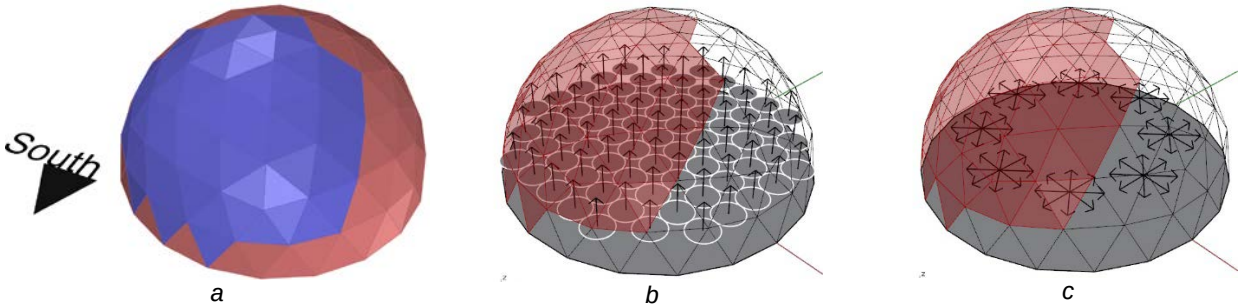

Figure 2: a) configuration corresponding to the chosen capacity PV covered part in blue(4.1 kW_{peak}), b) disposition of illuminance sensors for minimum threshold c) disposition of illuminance sensors for maximum threshold

The capacity chosen according to the previous method with the triangles sorted by irradiation leads to one single configuration [Figure 3a]. From the daylighting standpoint, the application of photovoltaics has a

considerable impact because completely opaque modules were used. Most of the dome surface available for transparent elements, so the main problem is not the lack of light, but the protection from glare, which causes discomfort. The spherical shape of the building rules out the possibility to apply a vertical opening, but creates some opportunities for a non-conventional, quality daylight. The dimension of the opening and its precise orientation are under investigation.

2.2.1 Daylight metrics

Verification of a sufficient light level in the space is performed through a similar procedure as above to measure the irradiation; here tough, the measured value is illuminance [Lux], and the simulation produces hourly values instead of cumulative ones. Using ray tracing for each time step would be computational demanding, therefore daylight coefficients applied for a discretized sky function [3] are used. This is implemented with the software tool Daysim. Once a threshold illuminance and an occupancy schedule are set, for each measuring point [Figure 3b] the percentage of hours in which the threshold is not met is calculated. The glare evaluation depends on the viewpoint of the observer and on a combination of sun position and weather condition. Most of the glare evaluation methods are picture based, i.e. they rely on a 180° picture to localize the light sources and measure their glare potential. The most used today is DGP (Default Glare Probability)[6]; this approach is reliable in predicting the response of the occupants, but requires a huge amount of calculations to verify the glare in a single point for a single hour, and is therefore computationally too costly for an annual assessment. A simplified version of the DGP formula is used [9] for visual comfort and energy analysis, this formula can be used under the conservative assumption that there is glare whenever direct sunlight hits the eye.

$$DGP_S = 6.22 \cdot 10^{-5} \cdot E_v + 0.184,$$

Equation 3: simplified default glare probability

where $\mathbf{DGP_S}$ is the value of probability of glare, is considered imperceptible<0.35, perceptible >0.35, disturbing>0.4 and intolerable ≥ 0.45; $\mathbf{E_v}$ is the illuminance on the vertical plane on the position of the eye. The formula above, differently from the original DGP, depends solely on the vertical eye illuminance and is known to fail on contrast based glare; more sophisticated approaches have been developed[5][10].

2.2.2 Optimization and Genetic algorithms

As the optimization is done using a genetic algorithm a numerical evaluation of the daylighting performance of the space is needed. An upper threshold to the vertical illuminance (on a set of viewpoints) of 3473 Lux, derived by [equation 3], can be set, providing a better prediction of the glare with no significant increase of the computational effort respect to an useful daylight illuminance (UDI)[4] approach. It was noticed that configurations with small openings, i.e. where contrast is common over high vertical illuminance[5], failed to provide adequate daylight, and so were discarded by the procedure. The minimum threshold was set on a series of horizontal illuminance measuring points [Figure 3b], while the maximum threshold was set on a sample of views [Figure 3c].

The part of the dome which is covered by PV is fully opaque, the rest was selected to be either transparent, or translucent (2% transmittance). The window is described by three angles: the first two are the polar coordinates on the dome; the third is its aperture with the center as a focus. These three angles are considered as “genes” in a genetic algorithm [11]; the algorithm randomly changes combinations of this three values and performs an annual daylight simulation to rate the performance of such combination. These ratings are used to select the best configurations. The simulation is a single target optimization. It is possible to separate the minimum illuminance performance from the glare performance and obtain a curve of optimal solutions containing various balances of these two fitness criteria. In this work, to avoid arbitrary choices at the end of the process, the two aspects were condensed in a ***DAI*** (daylight aggregated index)[Equation 4].

$$DAI = 1 - \left[0.5 \cdot \left(\frac{\sum_{a=1}^{n_{points}} \tau_E(a)}{n_{points}} + \frac{\sum_{b=1}^{n_{views}} \tau_G(b)}{n_{views}}\right)\right],$$

Equation 4:daylight aggregate index

where $\boldsymbol{\tau_E(a)}$ is the percentage of the time, over the total time of use of the building, when minimum illuminance (300 Lux) is not met on the specific a^{th} point**,** $\mathbf{n_{points}}$ is the total number of measuring points in the sample, $\boldsymbol{\tau_G(b)}$ is the percentage of time when maximum irradiance (3473 Lux) is exceeded on the specific b^{th} view while $\boldsymbol{n_{views}}$ is the total number of views in the sample.

2.3 Air and module temperature assessment

The thermal impact of the PV modules had to be estimated because a large portion of the incoming radiation is converted to heat. On a complex object as the dome, the use of building dynamic simulation tools is a limiting factor as the temperature distribution needs also to be assessed. The pattern of irradiation on a spherical surface would generate a particular gradient of temperature interacting with the heat exchange rate. The inside temperature and airflow is computed using the FEM software Elmer [7]. As boundary conditions for the computational fluid dynamic (CFD) simulation, temperature estimates were used. The problem with using boundary temperatures comes from the fact that, while it is used as an input for the CFD simulation, it is dependent on the internal temperature, which indeed is an output of the CFD. To find the envelope temperature a two-stage iteration was used. From the irradiation pattern, which can be calculated from weather data, a guessed inside temperature led to the initial surface temperature of the building envelope; afterwards the CFD analysis, using surface temperatures found before as a boundary condition, was used to find the inside temperature. The average inside temperature is then fed back into the next guess for the boundary conditions, and the process repeats until convergence.

2.3.1 Finding the module temperature / boundary condition

The temperature of the PV modules can be determined considering the heat flow of the total incoming power and the different loss mechanisms. The power transformed into heat is only the part of the irradiative power that is neither reflected nor converted into electricity [Equation 5].

$$G_{in} = G_{sol}(1-\rho)(1-\eta_{PV}),$$

Equation 5: heat gain of a module

where G_{in} is the heat gain of the surface G_{sol} is the incoming radiation, ρ is the reflectivity and η_{pv} is the efficiency of the PV module. To find the module temperature the loss mechanisms, i.e. convective and radiative heat transport, were considered [figure 2].

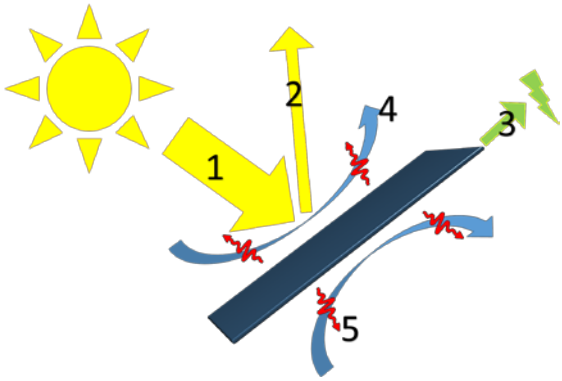

Figure 3: Energy flow in a PV module, showing the incoming radiative power (1), the reflected part of the light (2), convective cooling (4) and radiative heat losses (5). Conductive heat transport was neglected, as the contact area to the structure is small compared to the rest of the area and adjoining modules have a similar temperature, so the situation is assumed adiabatic.

The relevant loss mechanisms are convective and radiative. It was assumed, that the neighbouring modules are in a very similar condition and the small contact area between the modules can be assumed as adiabatic. The convective and radiative heat transport can be written as:

$$H_{conv/side} = h_{side}\left(T_{mod} - T_{air/side}\right),$$

and

$$H_{rad/side} = \varepsilon\sigma\left(T_{mod}^4 - T_{ground/sky}^4\right),$$

where $H_{conv/side}$ denotes the convective heat loss and $H_{rad/side}$ the radiative heat loss inside and outside of the dome respectively, h_{side} denotes the convention coefficient (inside/outside), T_{mod} denotes the module temperature, $T_{air,side}$ the air temperature on either interior or exterior, and $T_{ground/sky}$ the ground or sky temperature depending on the side of the module. ε is the emissivity and σ is the Stefan–Boltzmann constant. The incoming power is equal to the losses. Thus, the module temperature can now be determined via

$$G_{in} = H_{conv/outside} + H_{rad/outside} + H_{conv/inside} + H_{rad/inside}.$$

Equation 7: energy balance between gains and losses

However, the convective heat-transport coefficient h_{side} depends on the temperature of the air on that side of the dome using the Churchill and Chu correlation [12] and temperature dependence of the Rayleigh number [13]

$$h = \frac{k}{x}\left(0.825 + \frac{0.38\, Ra_x^{1/6}}{(1 + (0.492\, \alpha/\nu)^{9/16})^{8/27}}\right)^2,$$

Equation 9: churchill and Chu correlation

$$Ra_x = \frac{g\,\beta}{\nu\alpha}\,(T_{mod} - T_{air})x^3,$$

Equation 8:Rayleigh number

where ***x*** is the characteristic length of the problem , ***Ra$_x$*** is the Rayleigh number [*Equation 9*], ***k*** is the thermal conductivity, ***v*** is the kinematic viscosity of the fluid, ***α*** the thermal diffusivity and ***β*** the thermal expansion coefficient. The characteristic length is the depth of fluid involved in convection [14]. As an approximation, a value of one meter was used according to the dimensions of the dome. A sensitivity analysis for this parameter still needs to be done, but the temperatures found, relative to the incident radiations, were matched with experimental data [15].The gradient of solar irradiation was simplified by dividing it in discrete homogenous surfaces. Their width is chosen to evenly distribute the difference in irradiation.

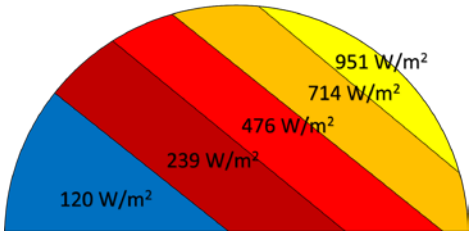

Figure 4 Simplified irradiance map used to find the boundary conditions.

For this simplified analysis, it was chosen that only the section with the highest irradiance values is equipped with PV modules. It is feasible to change this choice using the outcome of the optimization of section 2.1. The material constants where chosen as the ones of PVC coated polyester and PV module, respectively, and can be found in [Table 3].

Constant name	**Plastic / PVC-tent**	**Silicon / PV module**
k: thermal conductivity	0.23	0.23
ε : emissivity	0.84	0.95

Table 2:characteristics of the materials on the surface [16]

2.3.2 Computing the thermal flow in the dome

To find the thermal flow and the inside temperature of the dome the FEM analysis tool Elmer was used. It is based on heat and Navier-Stokes equations, which in turn can be derived from the basic principles of conservation of mass, momentum and energy[17]. The physical proprieties retrieved from the simulation are associated with internal points generated by the subdivision of the continuum of space in discrete tetrahedrons; the points are the extremes of each tetrahedrons. To calculate the average temperature every tetrahedron was given a temperature by averaging that of its four extreme points; as the tetrahedron volumes are strongly uneven, the mean, weighted on volume, of each tetrahedron's temperature was calculated. This mean temperature in turn was used as the next input to guess the envelope temperature, see section 2.3.1.

3. Results

3.1 Electricity production optimization

3.1.1 Input of the simulation

The irradiation data used as input in the simulation was recorded at the Bolzano airport weather station over one year. Shading was only considered from the horizon and near object shading was neglected. The main inputs are the following [Table 2].

PV system	**Energy price**
Efficiency 10%, Performance ratio 80% Degradation rate 1% (cigs [18]) Initial price 3000 €/kW$_{peak}$ [19] Maintenance costs 2%	Initial energy price 0.23 €/kWh [20] Energy price growth rate 2% [21]

Table 3: input used for production optimization

3.1.2 Output of the simulation

Provided that more irradiated spots are covered first, for this peculiar shape, but in general for every shape [22], the insolation and therefore the electric yield are negatively correlated to the area covered by PV, as on a building one needs to start covering north faces surfaces, and so to the peak capacity [Figure 2a)]. The second chart [figure 2b)] shows the NPV for different installed capacities and length of time installed. The maximum NPV in 20 years corresponds to a configuration slightly bigger than 4 kW$_{peak}$, in case of different needs (e.g. limited initial capital or high energy demand) the system shows a relative stability between 3 and 6 kW$_{peak}$. For the purpose of day lighting analysis the optimal solution (4.1 kW$_{peak}$) is chosen[Figure 3].

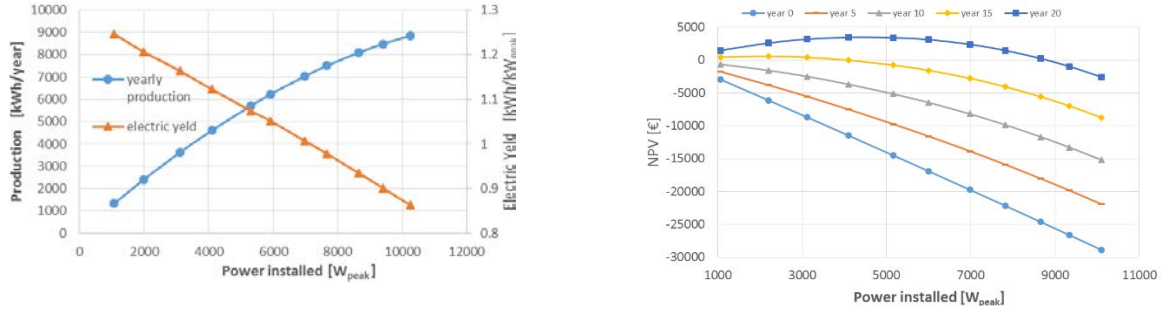

Figure 5: a) Production and yield versus capacity b) NPV at different time horizons versus capacity

3.2 Daylighting optimization

The output of the simulation is a list of many different configuration with their associated ***DAI***. A solution might be excellent in avoiding glare while blocking too much daylight or vice-versa without affecting the index. Strongly unbalanced Solutions (favoring light penetration or glare protection) are characterized by lower ***DAI***, while the best solutions are relatively balanced. The genetic algorithm, while trying to find the best configuration, sorts configurations from the best to the least performing one. In this example, the highest achieving configuration is shown in figure 4c), nevertheless not far down the list there is e.g. the solution shown in 4d) that, despite some small losses in ***DAI***, provides the possibility for the occupants to look outside. This gives the designers or architects some freedom and allows choosing the most esthetic solution from a number of optimal ones, or estimate the price in daylighting quality one has to pay in order to satisfy esthetic standards.

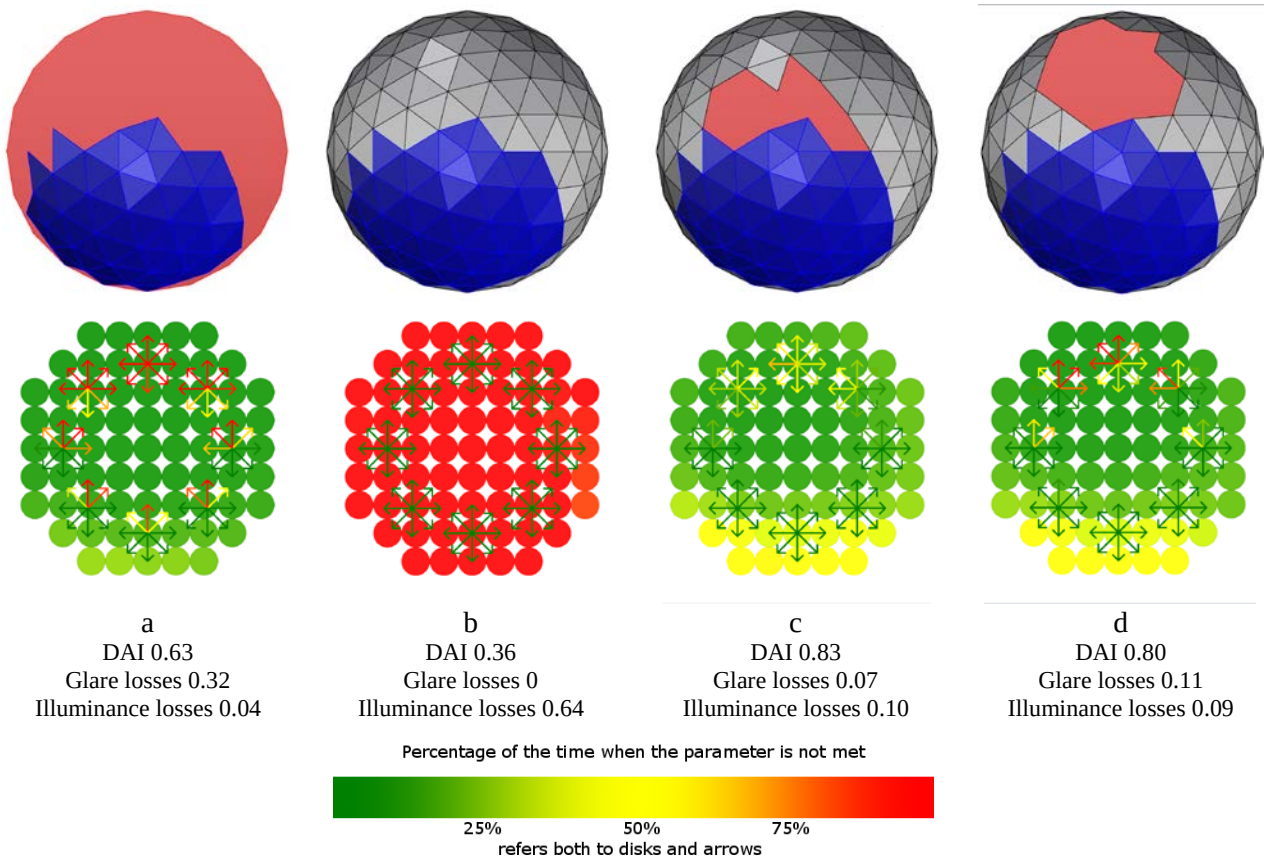

Figure 6: Graphical assessment of the performance of four configurations: PV part in blue, translucent part in grey, transparent part in red; illuminance associated colour on the disks, glare associated colour on the arrows.

3.3 Air and module temperature assessments

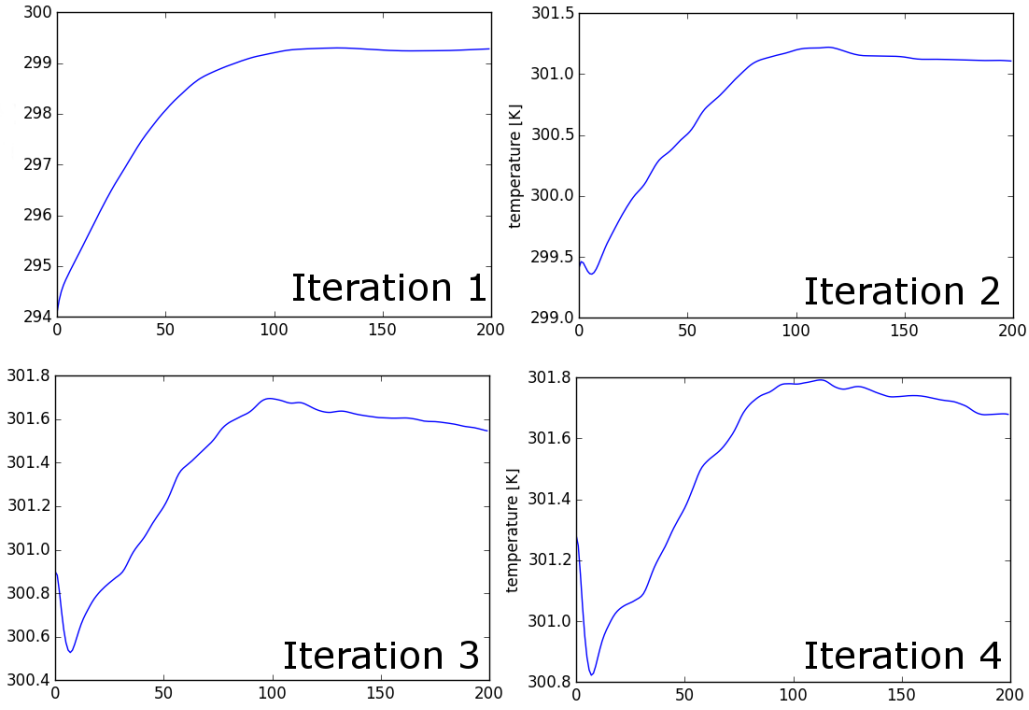

Figure 7: average temperature within the geodesic dome over time (200 seconds)

Given the outside conditions (Direct normal Radiation 950 W/m^2, Diffuse Horizontal 120 W/m^2, ground temperature 293.15°K-20°C and dry bulb air temperature 298.15°K-25°C) a low initial guess internal temperature was chosen to examine the process of convergence. Given a convergence factor of 0.2°C the internal temperature converged at 301.7°K within four iterations [Figure 7]. From [Figure 8 a)] the formation of a convective pattern within the dome is apparent, the air movement seems to involve mostly the upper part of the building. the air velocities are below 1.5 m/s. in [Figure 8 b]] the temperature gradient inside the dome is shown during the 200th second: there are some pockets of extreme temperatures (> 313.15°K-40°C), but they remain confined in the upper part of the structure, above 2.15 meters.

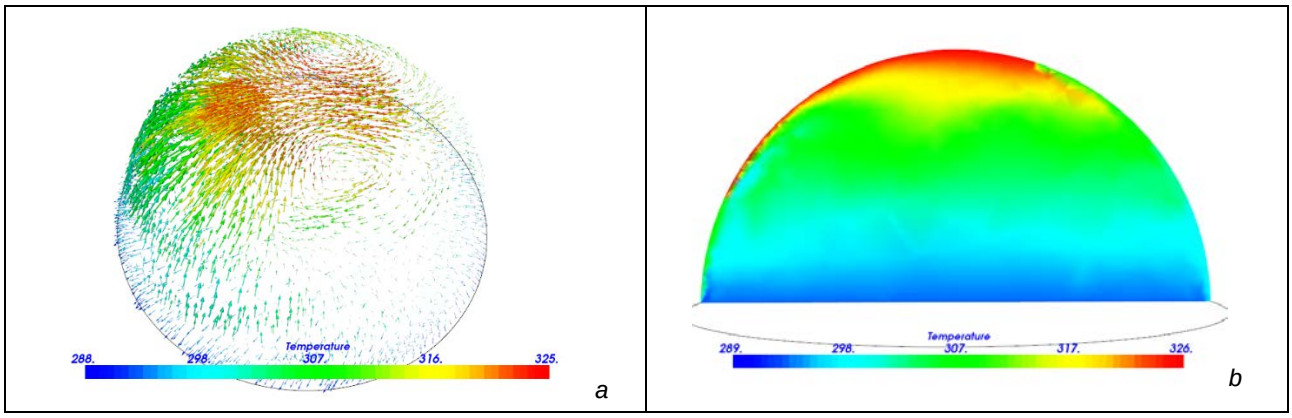

Figure 8: graphical visualization of the convection a) and the temperature gradient inside the dome b).

4. Conclusions

In the first part of the study, the financial examination shows that there is a wide range of PV configurations that will still provide a near maximal NPV. Thus, it gives a certain freedom to the architects and financer to choose with which configuration to equip the building. The largest installed system is 6kW$_{peak}$ and can be seen as the building´s PV potential. In the daylighting analysis a single parameter is used to rate the daylighting and glare performance of a geometrical space from yearly weather data. Again, the optimization does not give one perfect solution but leaves the designer / architect a certain degree of freedom to incorporate esthetical as well as functional aspects of the building. In the last part, the thermal analysis, it was possible to predict the inside temperature without artificial cooling. In this case it was found that the lower part, less than 2.5 meters (occupant's level), stays at a temperature of 25°C, which is at comfort level. Considering the costs of creating a mock-up of the building, the CFD will be compared with another one modelling an air depth outside the dome and using energy flow instead of temperatures; the temperature approach should be also examined in ventilated facades and compared with both existing methods and experimental data.

The method proposed in this work consists essentially in the combination of existing and well proven techniques with some adaptations, therefore the results, given the quality of the inputs, can be trusted. Nevertheless, the method needs to be proven experimentally. Further, a sensitivity study for the important input parameters has still to be done. This building exemplifies how BIPV has consequences on many physical and comfort parameters. The method helps to access such parameters and, in some cases, allow for optimization.

The aim was to provide a tool that helps architects and designers to understand the impact of the integration of PV and encourage the designer to use PV in a way that benefits the whole building system. A better performance of the systems can be achieved thanks to the combined simulation of all the effects. Rather than analysing only one of the aspect, the interactions between these different subsystems are shown in a synthesized way.

Furthermore, the method is based purely on open source software. Which is especially important to promote these studies and make them widely available among students and small enterprises.

This work is a first step toward a software tool specialized in BIPV which will provide architects with useful insights and optimization procedures on the impact of BIPV on the building physics and on the energy production.

5. Aknowledgements

This paper was produced within the framework of SolarDesign Project (SolarDesign Project has received funding from the EU's Seventh Framework Programme (FP7/2007-2013) under grant agreement n° 310220) and within the framework of Flexi-BIPV, financed by the ERSF Programme of the Province of South Tyrol (Project 5-1a-232).

6. References

[1] K. Fath, J. Stengel, W. Sprenger, H. R. Wilson, F. Schultmann, and T. E. Kuhn, "A method for predicting the economic potential of (building-integrated) photovoltaics in urban areas based on hourly Radiance simulations," *Sol. Energy*, vol. 116, pp. 357–370, Jun. 2015.
[2] Grynberg Anat, "Validation of RADIANCE." Lawrence Berkeley Laboratory, Applied Sciences Division, Lighting Systems Research Group, 1989.
[3] C. F. Reinhart and S. Herkel, "The simulation of annual daylight illuminance distributions — a state-of-the-art comparison of six RADIANCE-based methods," *Energy Build.*, vol. 32, no. 2, pp. 167–187, Jul. 2000.
[4] A. Nabil and J. Mardaljevic, "Useful daylight illuminances: A replacement for daylight factors," *Energy Build.*, vol. 38, no. 7, pp. 905–913, Jul. 2006.
[5] J. Y. Suk, M. Schiler, and K. Kensek, "Development of new daylight glare analysis methodology using absolute glare factor and relative glare factor," *Energy Build.*, vol. 64, pp. 113–122, Sep. 2013.
[6] J. Wienold and J. Christoffersen, "Evaluation methods and development of a new glare prediction model for daylight environments with the use of CCD cameras," *Energy Build.*, vol. 38, no. 7, pp. 743–757, Jul. 2006.
[7] "CSC - Elmer." [Online]. Available: https://www.csc.fi/web/elmer/elmer. [Accessed: 24-Jun-2015].
[8] P. R. Tregenza, "Subdivision of the sky hemisphere for luminance measurements," *Light. Res. Technol.*, vol. 19, no. 1, pp. 13–14, Jan. 1987.
[9] J. Wienold, "dynamic simulation of blind control strategies for visual comfort and energy balance analysis." 2007.
[10] S. Kleindienst and M. Andersen, "The Adaptation of Daylight Glare Probability to Dynamic Metrics in a Computational Setting," *Proc. Lux Eur. 2009 – 11th Eur. Light. Conf.*, 2009.
[11] L. Sean, *Essentials of Metaheuristics*. Lulu, 2013.
[12] S. W. Churchill and H. H. S. Chu, "Correlating equations for laminar and turbulent free convection from a horizontal cylinder," *Int. J. Heat Mass Transf.*, vol. 18, no. 9, pp. 1049–1053, Sep. 1975.
[13] M. Favre-Marinet and S. Tardu, "Forced Convection Around Obstacles," in *Convective Heat Transfer*, ISTE, 2009, pp. 119–139.
[14] B. Kozanoglu and F. Rubio, "The characteristic lenght on natural convection from a horizontal heated plate facing downwards," *Therm. Sci.*, vol. 18, no. 2, p. 555, 2014.
[15] L. Maturi, G. Belluardo, D. Moser, and M. Del Buono, "BiPV System Performance and Efficiency Drops: Overview on PV Module Temperature Conditions of Different Module Types," *Energy Procedia*, vol. 48, pp. 1311–1319, 2014.
[16] B. Lee, J. Z. Liu, B. Sun, C. Y. Shen, and G. C. Dai, "Thermally conductive and electrically insulating EVA composite encapsulants for solar photovoltaic (PV) cell." 2008.
[17] P. Råbac, M. Malinen, J. Ruokolainen, A. Pursula, and T. Zwinger, "Elmer Models Manual," in *Elmer Documentation*, .
[18] D. C. Jordan and S. R. Kurtz, "Photovoltaic degradation rates—an analytical review," *Prog. Photovolt. Res. Appl.*, vol. 21, no. 1, pp. 12–29, 2013.
[19] G. Verberne, P. Bonomo, F. Frontini, M. N. van den Donker, A. Chatzipanagi, K. Sinapis, and W. Folkerts, "BIPV Products for Façades and Roofs: a Market Analysis." 2014.
[20] eurostat, "Half-yearly electricity and gas prices, second half of year, 2012–14 (EUR per kWh)." .
[21] W. R. E. INTELLIGENT ENERGY EUROPE, "Electricity prices scenarios until at least the year 2020 in selected EU countries." Jan-2012.
[22] P. Redweik, C. Catita, and M. Brito, "Solar energy potential on roofs and facades in an urban landscape," *Sol. Energy*, vol. 97, pp. 332–341, Nov. 2013.
